3D Modelling of the Wind Flow Trajectories and Its Characteristic Effects on Horizontal Axis Wind Turbine at Different Wind Regimes

Etuk Ekom Mike[1, *], Ikpe Aniekan Essienubong[2]

[1]Department of Production Engineering, University of Benin, Benin City, PMB 1154, Nigeria; [2]Department of Mechanical Engineering, University of Benin, Benin City, PMB 1154, Nigeria

Abstract: In this study, an overview of the effect of turbulence on wind turbine performance is presented. Flow Models with full description were generated to clearly illustrate Winfield plots, 3 Dimensional Spatial Wind Flow Directions, Wake Distribution Patterns behind the Rotors, and 3 Dimensional Spatial Turbulent Wind Distribution Patterns. The power and the coefficient of power were examined from the wake vortex simulation while the flow velocity cut plots at different wind speeds (2, 4, 6 and 8 m/s) and time steps (2, 4 and 6 s) were obtained using Q-Blade software. The results revealed that, while the power coefficient was observed to decrease and increase with increasing wind speed, the power output increased variably from 0.0416903 to 2.51354 kw as the wind speed also increased from 2 to 8 m/s at peak time step of 6s. It was also found that, while the wind influx towards a wind turbine can be displaced by extreme turbulence which subsequently displaces the wind directions, reduces turbine trust, power coefficient and the power output; the wake effect downstream can affect the wind speed and performance of other turbines downwind. The characteristics and complexity of a given terrain as well as the aforementioned factors should be considered while siting and operating a wind turbine or wind farm.

Keywords*: Modelling, Wind flow, Wind turbine, Wake vortices, Turbulence, Wind direction,*

Introduction

Atmospheric wind flow has a strong turbulence fluctuation and shows transient characteristics (Kim & Kim, 2012). Upon approaching a wind turbine, the wind speed decreases and turbulence increases. Consequently, rotation of the wind turbine blades results in turbulence, manifesting in the form of rotational vertical wakes which are sustained behind the rotors in a distance for several miles before being dissipated fully (Brand *et al*., 2011). The turbulence in the flow towards a wind turbine is modelled on the basis of similarity theory in combination with computational fluid dynamics (CFD) methods (Satoh, 2004). Mikkelsen (2013) investigated the effect of free stream turbulence on a model wind turbine's performance characteristics and the wake development downstream using a reference wind speed of 10 m/s. The wind turbine was found to operate most efficiently at TSR≈6, the peak power coefficient (C_p) without free stream turbulence was 0.461, while C_P of 0.45 was obtained with free stream turbulence. Hence, the power coefficient seemed to be slightly reduced with increased levels of turbulence, except at low tip speed ratios where the effect of stall dominated.

The effects of wind shear and inflow turbulence on the performance of a semisubmersible offshore floating wind turbine was investigated by Li *et al*. (2018). It was observed that the ultimate structural and fatigue damage loads at the blade root were augmented by inflow turbulence and wind shear. Both the ultimate and fatigue damage loads increased as a result of inflow turbulence and wind shear. The effect of inflow turbulence on the power generation was observed to depend on the operational state due to the control scheme of the wind turbine.

Existing wind farm wake models vary from low-fidelity empirical and semi-empirical approaches (Ainslie, 1988), to more complex high fidelity large-eddy simulations where the turbines are parameterized using either an actuator disc (Jimenez, 2007), or an actuator line approach (Troldborg *et al*., 2010, Troldborg *et al*., 2011). Actuator disk (Sanderse, 2000), and actuator line (Troldborg *et al*., 2010), methods have been employed in simulating the rotor and aerodynamic flow around a wind turbine by solving the NS equations, which enabled the CFD domain to cover the region extending from the

---

Corresponding: E-Mail: alwaysetuk@gmail.com; Tel: +2348025276325; Fax: +23452602361

rotor plane to several diameters downstream, and to fully compute the near and far vortex wake elements.

Wußow et al. (2007) employed CFD model (ANSYS FLUENT 6.3 using the LES technique) to simulate a full meandering turbulent wake using an incoming wind field that matches the IEC-61400 requirements. Tip or nacelle vortices were only slightly present in the near wake region which was observed to meander horizontally and vertically. The relatively high velocity gradients experienced at either the outer and inner edges of the wake in conjunction with the meandering contributed significantly to the turbulence intensity observed on a ten-minute time scale. Zhang *et al*. (2012) investigated the near-wake flow structure downwind of a wind turbine in a turbulent boundary layer, and observed that the significant turbulence enhancement at a distance of three rotor diameters is associated with strong wind shear and high mechanical production of turbulent kinetic energy at the top-tip level. The spatial distribution of vorticity and swirling strength measured with High-resolution particle image velocimetry (PIV) also revealed the presence of top-tip vortices, which persist up to about 2-3 rotor diameters downwind of the turbine, longer than the hub/root vortices in the near wake region. The measurements also revealed intense flow rotation and a highly non-axisymmetric distribution of the mean flow and turbulence structure in the near wake.

In an experimental investigation conducted by Ozbay *et al*. (2016), on wake characteristics and aeromechanics of Dual-Rotor Wind Turbines, the vortex structures were found to move outward with the expansion of the wake flow as they moved downstream, and finally merged with the tip vortex structures and eventually dissipated further downstream. In an experimental study on the evolution of unsteady wake vortex structures in turbine wake flows, Tian *et al*. (2014), Hu *et al*. (2012), and Whale *et al.* (2000) also observed related vortex structures at approximately 50-60% span of the rotor blades. In this study, wind flow trajectories, wind field regime and characteristics were modelled at various wind speeds, and their effects on horizontal axis wind turbine performance were examined.

Materials and Method

The flow around a rotor blade is modelled by using blade element/momentum theory and employing sectional airfoil data (Sørensen, 2011). The airfoil data have been found to depend heavily on unsteady flow (Devinant *et al*., 2002). The airfoil data is practically obtained from a wind tunnel experiments but can also be obtained through conventional methods such as computational fluid dynamics or aerodynamic design methods. In this study, the flow around a rotor blade was modelled using blade element/momentum theory embedded in QBlade software. A generator for turbulent windfields and module to generate a simplified structural model is integrated in QBlade v0.8 which was used to setup a FAST unsteady aeroelastic simulation reported in this study. Turbulent Windfield Generator which is a submodule of QBlade uses the Sandia Method to create turbulent windfield. The QBlade simulation interface is presented in Figure 1.
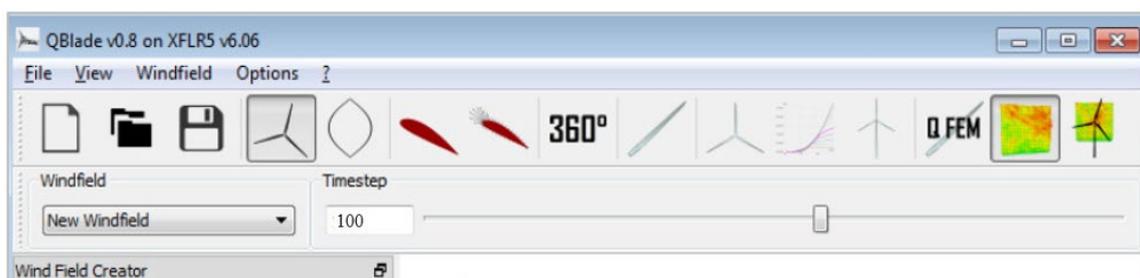
Figure 1. QBlade simulation interface

The windfield objects generated were further used in a FAST simulation. From inside the FAST module, aeroelastic FAST simulation was set up, simulated and post processed from QBlades internal database. To setup a FAST simulation for the windfield, details of the rotor, simulation parameters, windfield parameters and the blade structure were specified in the Parameter tab as shown in Table 1. This enabled the visualization of different time steps using the slider inside the toolbar.

Table 1. Flow parameters employed in the wind field simulation

Wind field Parameter	Simulation Parameter	Wind Field Properties	Environment
Time: 60s	Hub Height: 15 m	2 m/s	Gravity: 9.81 m/s²
Time steps: 100	Measurement Height: 15 m	4 m/s	Air Dens: 1.225 k/m³
Points per direction: 40	Turbulence Intensity: 5%	6 m/s	Kin Visc: 1.4661e-05 m/s
No of blades: 3	Include Shear Layer: True	8 m/s	
Nacelle Yaw: 0 Deg.	Roughness Length: 1e-02 m		

The degrees of freedom of the structural model (FlapDOF 1&2, EdgeDOF) was enabled in order to effectively observe the simulation iterations through visual process. The simulation was initiated by pressing the start simulation button from the dock. When the simulation was completed, the FAST results were automatically loaded inside QBlades database for observation. The theory and mathematical formulations upon which the simulation in this study is based are already embedded in the software, and can be expressed in the following Equations:

Reynolds number which is considered as the inertial forces divided by viscous forces is given by Equation 1.

$$Re = \frac{U_\infty D}{v_w} \tag{1}$$

where U_∞ is the free stream velocity, D is the turbine diameter and v is the wind viscosity. The chord Reynolds number Re_c is the same as Equation 1, with the blade chord length c being the characteristic length scale:

The kinetic energy of an air mass m moving at a velocity U can be expressed as:

$$E = \frac{1}{2}mU^2 \tag{2}$$

The mass flow rate of air with density p, passing through the rotor cross-sectional area A is given by Equation 3 while the power available in the air stream is expressed in Equation 4.

$$\dot{m} = \rho UA \tag{3}$$

$$P = \frac{1}{2}\rho U^3 A \tag{4}$$

The lift and drag coefficients, based on the lift L and drag D per unit length are given by Equation 5 and 6.

$$C_L = \frac{L}{\frac{1}{2}\rho U_{rel}^2 c} \tag{5}$$

$$C_D = \frac{D}{\frac{1}{2}\rho U_{rel}^2 c} \tag{6}$$

where U_{rel} and c denotes the chord length. The relative wind velocity U_{rel} expressed in Equation 7, is the relative velocity between the axial velocity U and the rotational velocity $r\Omega$ at the local intermediate radius r. The solidity σ of a turbine at a radial position r is given by Equation 8.

$$U_{rel}^2 = U^2 + (r\Omega)^2 \tag{7}$$

$$\sigma(r) = \frac{c(r)B}{2\pi r} \tag{8}$$

where B is the number of blades. The total solidity can then be found by integrating Equation 8 along the blade radius. According to Fukumoto & Okulov (2005), Wind turbine wakes are modelled as helical vortices which represents the region where the flow is spinning about an axis. Figure 2 shows the cross sectional view of a helical vortex around a wind turbine rotor.

In a cylindrical coordinate system, the velocity field is described (Zheng & Wu, 2018) as follows:

$$u_\rho = \frac{\Gamma}{2\pi\rho l} \sqrt[4]{(l^2+\rho^2)(l^2+a^2)} Im\left\{\frac{e^{ix}}{e^{\pm\xi}-e^{ix}} \pm \frac{l}{24}\left[\frac{2l^2+9a^2}{(l^2+a^2)^{3/2}} - \frac{2l^2+9\rho^2}{(l^2+\rho^2)^{3/2}}\right] log\left(1-e^{\pm\xi+ix}\right)\right\}, \tag{9a}$$

$$u_z = \frac{\Gamma}{2\pi l}\left\{\begin{matrix}1\\0\end{matrix}\right\} + \frac{\Gamma}{2\pi l}\frac{\sqrt[4]{(l^2+a^2)}}{\sqrt[4]{(l^2+\rho^2)}} Re\left\{\frac{\pm e^{ix}}{e^{\pm\xi}-e^{ix}} + \frac{l}{24}\left[\frac{3\rho^2+2l^2}{(l^2+\rho^2)^{3/2}} + \frac{2l^2+9a^2}{(l^2+a^2)^{3/2}}\right] log\left(1-e^{\xi+ix}\right)\right\}, \tag{9b}$$

$$u_\phi = \frac{\Gamma}{2\pi l} - \frac{lu_z}{\rho} \tag{9c}$$

where u_ρ, u_z and u_ϕ are the velocities in *p, z* and *ϕ* coordinates in Figure 2, Γ is the circulation of the vortex filament and α is the radius of the helical vortex. To avoid singularity at the mid-section of the helical vortex filament which may result in overestimated velocity values in the airflow close to the vortex centre, flow velocity around the helix is modelled as the rotation core axis (Fukumoto & Okulov, 2005, Mulinazzi & Zheng, 2014).

Figure 2. Cross sectional view of a helical vortex around a wind turbine rotor

$$v = \frac{\Gamma}{2\pi\sigma^2}\alpha \qquad (10)$$

Where σ is the core size of the helical vortex. Conservation of momentum and mass for the helical control volume with a cross section shown in Figure 2 are given by Equation 11 and 12 (Odemark, 2012).

$$\rho u_1^2 + \rho u_\infty^2(A_0 - A_1) + \dot{m}_{side}U_\infty - \rho U_\infty^2 A_0 = -T \qquad (11)$$

and

$$\rho u_1 A_1 + \rho U_\infty(A_0 - A_1) + \dot{m}_{side} = \rho U_\infty A_0 \Rightarrow \dot{m}_{side} = \rho A_1(U_\infty - u_1) \qquad (12)$$

Mass conservation is also expressed as:

$$\dot{m} = \rho u A = \rho u_1 A_1 \qquad (13)$$

Combining Equation 11-13 yields:

$$T = \rho u A(U_\infty - u_1) = m(\overset{.}{U_\infty} - u_1) \qquad (14)$$

where U_∞ is the free stream velocity (upstream), u_1 is the wind velocity downstream, T is the thrust force, A is the rotor area, ρ is the air density, $\dot{m}_{side}$ and m are the total mass flow out of the surface area. The wind velocity at the rotor plane is the mean between the velocity far upstream and downstream, and can be expressed as:

$$u = \frac{1}{2}(U_\infty - u_1) \qquad (15)$$

By defining a control volume following the streamlines and applying the conservation of energy, the following relationship for the power P is found (Odemark, 2012).

$$P = \dot{m}\left(\frac{1}{2}U_\infty^2 + \frac{\rho_\infty}{\rho} - \frac{1}{2}u_1^2 - \frac{\rho_\infty}{\rho}\right) \Rightarrow P = \frac{1}{2}\rho U A(U_\infty^2 - u_1^2) \qquad (16)$$

where ρ_∞ is the free stream static pressure. By introducing the axial induction factor a and applying Equation 15, the power and the thrust forces can be expressed as:

$$P = 2\rho U_\infty^3 a(1-a)^2 A \qquad (17)$$

and

$$T = 2\rho U_\infty^2 a(1-a) A \qquad (18)$$

where the axial induction factor a is given by Equation 19 while the angular induction factor a' is defined by Equation 20.

$$a = \frac{U_\infty - u_1}{U_\infty} \qquad (19)$$

$$a' = \frac{\omega}{2\Omega} \qquad (20)$$

where Ω denotes the angular velocity of the wind turbine rotor, and ω is the angular velocity imparted to the flow stream. The dimensionless power and thrust coefficients thus become:

$$C_P = \frac{P}{\frac{1}{2}\rho U_\infty^3 A} = 4a(1-a)^2 \qquad (21)$$

and

$$C_T = \frac{T}{\frac{1}{2}\rho U_\infty^2 A} = 4a(1-a) \qquad (22)$$

The tip speed ratio (TSR) λ is the ratio between the rotational velocity at the tip of the blade and the free stream velocity U_∞, expressed in Equation 23:

$$\lambda = \frac{\Omega R}{U_\infty} \tag{23}$$

Using the energy equation on a control volume that moves with the blade, the pressure difference across the blade can be expressed as (Manwell et al., 2009):

$$p_2 - p_3 = \rho \left(\Omega + \frac{1}{2}\omega \right) \omega r^2 \tag{24}$$

where ω is the angular velocity and R is the rotor radius. Applying Equation 20, 23 and 24, the thrust on an annular element can be expressed in Equation 25.

$$dT = 4a'(1 + a')\frac{1}{2}\rho\Omega^2 r^2 2\pi r dr = 4a(1 - a)\frac{1}{2}\rho U^2 2\pi r dr \tag{25}$$

The torque Q, exerted on the blade, is equal to the change of angular momentum of the wake. Therefore, the torque for an incremental annular area element, is given by Equation 26.

$$dQ = d\dot{m}(wr)r = 4a'(1 - a)\frac{1}{2}\rho U\Omega r^2 2\pi r dr \tag{26}$$

The instantaneous wind speed in the three dimensions u, v and w can be defined as,

$$u_1 = U_\infty + u_1' = \bar{u}_1 + u_1' \tag{27a}$$
$$v = V + v' = \bar{v} + v' \tag{27b}$$
$$w = W + w' = \bar{w} + w' \tag{27c}$$

The characterization of turbulence may be by a relatively constant short-term mean, with fluctuations about the mean, and the probability density function that best describes the type of behaviour for turbulence is the Gaussian distribution expressed as:

$$f(u_1) = \frac{1}{\sigma_u\sqrt{2\pi}} exp\left[-\frac{(u_1 - U_\infty)^2}{2\sigma^2_{u_1}} \right] \tag{28}$$

Turbulence intensity in the streamwise direction is given by Equation 29.

$$T_u = \frac{\sigma_u}{U} \tag{29}$$

where σ_u is the standard deviation of wind speed variations about the mean wind speed U.

Using the mean turbulent normal stresses $\bar{u}_1'$, kinematic viscosity v' and the rotational speed of wake w', the turbulent kinetic energy can be quantified as:

$$k = \frac{1}{2}(\bar{u}_1'\,\bar{u}_1') + (\overline{v'\,v'} + \overline{w'\,w'}) \tag{30}$$

The equation for the evolution of turbulent kinetic energy is expressed as:

$$\frac{Dk}{Dt} + \nabla.T' = P - \epsilon \tag{31}$$

where $\nabla.T'$ is the turbulent transport or turbulent diffusion, P is the production of turbulent kinetic energy (the source) and ϵ is the dissipation of turbulent kinetic energy.

Windfield Plots

Modelling of wind field is an important aspect of wind turbine blade related studies, as it provides images as well as animated visuals of how the wind velocity impacts forces on the rotor blade to cause its rotation. To understand the interplay between the rotor blade and its driving mechanism, wind field must be modelled to effectively represent the wind speed range in the domain intended for the rotor blade to perform. The flow field around a wind turbine may be characterized by two major mechanisms including convection and turbulent diffusion (Vermeer et al., 2003). In this study, the wind field plots as shown in Figure 3a-d represents the distribution of surface plot of the wind perpendicular to the turbine axis. All wind heights are taken at 15m and a constant turbulence of 5%. A wind shear of 0.001m is assumed for all wind fields. The simulation was run for 60s and results are shown at a time step of 100. The wind measurement height was at 15m from sea level.

Cold air which is denser, sinks to the ground because the air molecules are too heavy to soar higher in the atmosphere while hot air which is less dense rises and in the process circulates across the atmosphere. The air circulation process may be referred to as "Wind" because it is characterized by a current of air flowing in various directions across the earth's surface.
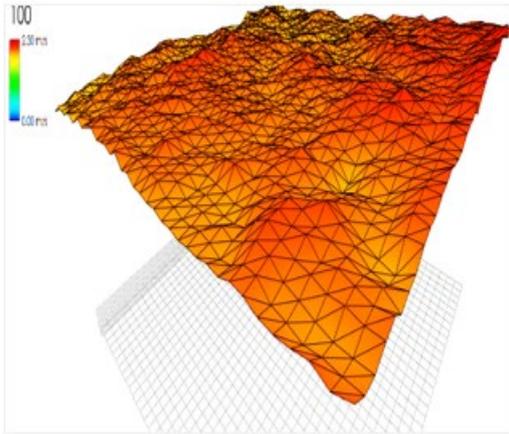
Figure 3a. Winfield plot at mean wind speed of 2 m/s   **Figure 3b**. Winfield plot at mean wind speed of 4 m/s
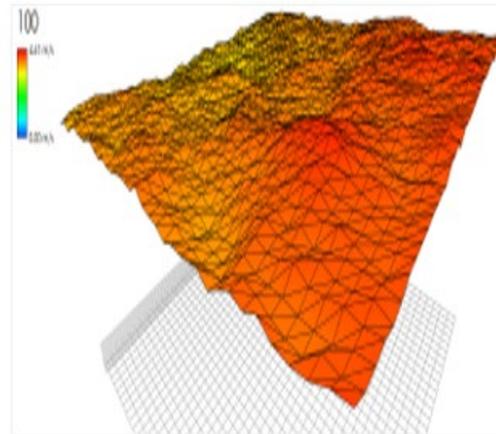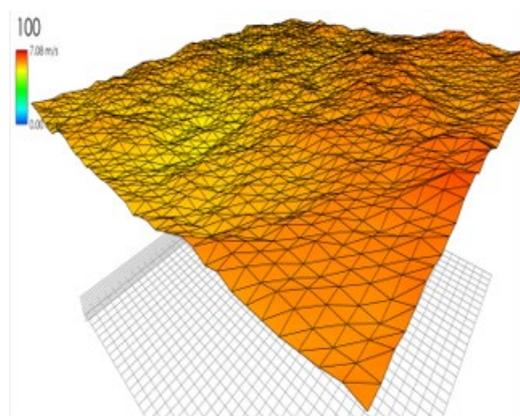
Figure 3c. Winfield plot at mean wind speed of 6 m/s   **Figure** 3d: Winfield plot at mean wind speed of 8 m/s
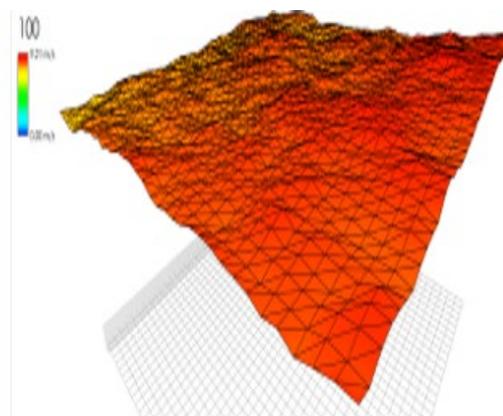
Generally, wind direction which is usually parallel to isobars due to earth's rotation may also be horizontally transverse such that it either flows sideward from the direction it originates towards an angle ranging from 0°- 360° and across the windfield as shown in Figure 4a-b, or may occur in the vertically transvers direction as shown in Figure 4c-d. It should be noted that the rotational speed of a given turbine blade is highly dependent on not only the wind speed but also on the wind direction. Therefore, if the maximum wind flow is not towards a direction suitable enough to cause the wind turbine rotor blade to attain its optimum speed, the wind turbine may perform below the expected capacity. Hence, it is necessary for the wind direction in a particular region to be studied extensively before mounting the wind turbine as well as its blades, as this can provide useful information on the angle of attack or angle of incidence and the direction to which high velocity magnitude gradient/maximum wind speed is expected.
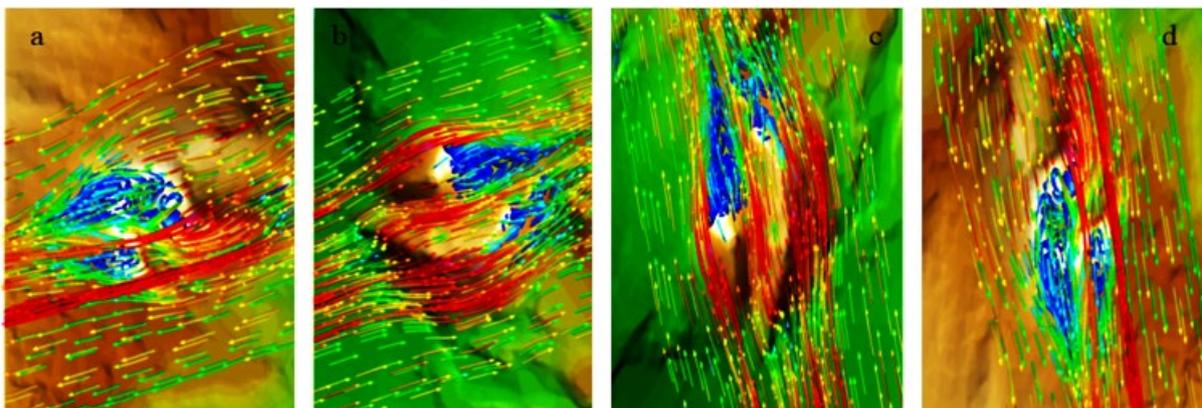
Figure 4. 3 Dimensional Spatial Wind Flow Directions

The wind flow regime as observed in Figure 4a-d, shows a network of wind current that is distributed across a given flow path. This is independent on the wind speed and dependent on the flow direction which usually produce an aerodynamic wake region downstream from the rotor blade. There are two major occurrences that take place during the operation of a wind turbine and rotation of its blade along the axis. First, the turbine extracts energy from the windfield and in the process reduces the wind speed. Second, turbulence is created in the air passing through the rotor blades which is then carried downwind. In other words, the region at which wind flow recirculates downstream or immediately behind the rotating blades which may be accompanied by flow separation and turbulence is known as wake. The wake region is generally associated with some aerodynamic characteristics such as velocity deficit, pressure differential, flow expansion, rotation of the wake field and increased turbulence. (Mckay et al., 2012). The theory of wind turbine wakes is classified into two categories namely: near wake and far wake. The near wake region deals with the extraction of energy from the wind by a single turbine, whereas, the far wake is more particular about the effects on the downstream turbines (Marmidis et al, 2008). Zhang et al. (2012) observed that, while the wind turbine extracts momentum from the flow and induces rotation, the stream-wise velocity decreases significantly and the lateral and vertical velocities increase immediately behind the rotor. In addition, the wake grows with increasing downwind distance from the rotor, as the stream-wise velocity increases and the other velocity components decrease. As the wind flow proceeds downstream the wake spreads in a non-uniform pattern as shown in Figure 5 but recovers towards free stream condition. The aerodynamic force driving the rotors result in an opposing force on the air stream causing the air column to rotate. The low pressure column of rotating air expands as it flows downstream of the turbine blades and consequently dissipates as the surrounding airflow reaches equilibrium (McKay et al., 2011, Burton et al., 2001). In event of a single wind turbine unit, the aforementioned wake does not have any effect on the wind turbine. However, in the event of a windfarm which consists of multiple stands of wind turbine, wake may have a cascading effects on a number of wind turbines in the farm. The wake effect becomes the aggregated influence on the energy produced from a wind farm due to the variations in wind speed as a result of the turbine impact on one another. In this case, each turbine unit extracting energy from the wind domain causes a reduction in the wind speed flowing to the next unit, increases vibration due to turbulence, increases wear around contacting members and increases maintenance cost. The radius of wake effect region downwind the rotors x, can be expressed as (Li et al., 2017):

$$R_w = \left(\frac{35}{2\pi}\right)^{\frac{1}{5}} (3c_1^2)^{\frac{1}{5}} (C_T A x)^{\frac{1}{3}} \tag{32}$$

$$c_1 = l(C_T A x)^{-\frac{1}{3}} \tag{33}$$

The wind speed reduction ΔU is described as:

$$\Delta U = -\frac{U_{WT}}{9} (C_T A x^{-2})^{\frac{1}{3}} \left[R_w^{\frac{3}{2}} (3c_1^2 C_T A x)^{-\frac{1}{2}} - \left(\left(\frac{35}{2\pi}\right)^{\frac{3}{10}} (3c_1^2)^{-\frac{1}{3}} \right) \right]^2 \tag{34}$$

where A is the swept area, T_C is the thrust coefficient, c_1 is constant, U_{WT} is the average wind speed on the wind turbines' hub height. Turbulent flow patterns in the incoming wind are rotationally sampled by the rotor blade. The turbulence in each section of the rotor blade is modelled on the basis of a spectrum (Kaimal et al., 1972), in combination with inverse Fourier transforms (Veers, 1984) or an approach based on rapid distortion theory (Mann, 1998).

As mentioned earlier, turbulence is created in the air flowing through the rotor blades as it rotates along its axis. Turbulent flow is a set of seemingly random and continuously changing wind motions that are superimposed on the wind's average motion. As shown in Figure 6, it is characterized by irregular swirls or fluctuations in the wind flowing towards and across the wind rotors, and is quantified with a metric known as turbulence intensity. An increase in downstream turbulence is caused by wake rotation, disruption of the air flow across the rotor blades and the vortices formed at the blade tips. This results in variation in wind speed and increased displacement in wind direction, causing less power being available for the downstream turbines (Mckay *et al.*, 2012). The incoming turbulent flow causes the flow field in the boundary layer around the blades to transform rapidly into a turbulent boundary layer. This increases the boundary layer thickness as indicated by the red regions in Figure 6 and hence, the drag also. Effect of increased turbulence may result in increase in the power present in the wind while drag forces may act negatively against it. This correlates with the findings of Mikkelsen (2013)

who reported that turbulence increases the relative velocity of the wind which in turn increasing the power extraction. However, at extremely high turbulence, wind direction may be displaced, leading to decrease in the velocity of wind flowing towards the turbine rotors which consequently result in the reduction of power output.
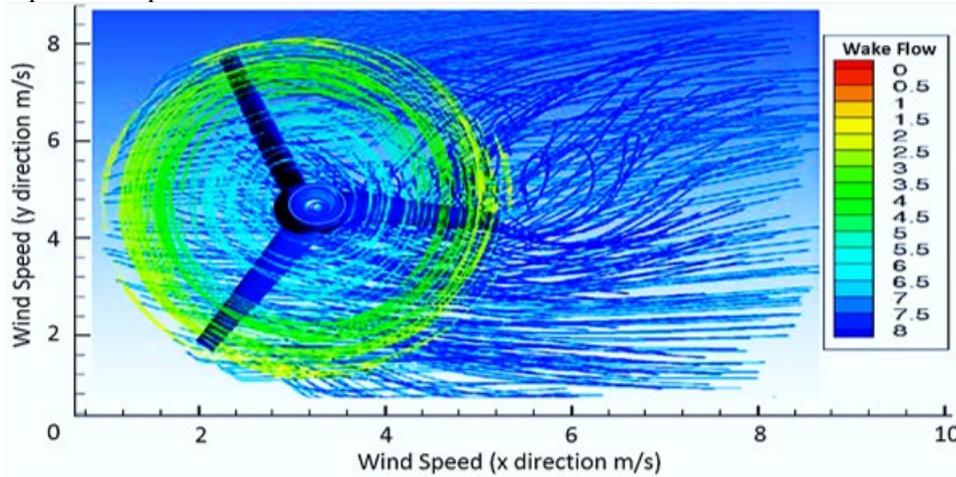
Figure 5. Wake distribution patterns behind the rotors
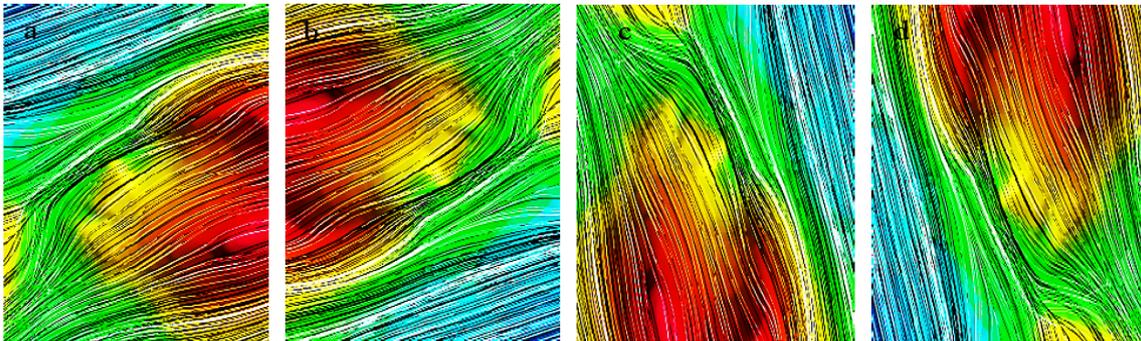
Figure 6. 3 Dimensional Spatial Turbulent Wind Distribution Patterns

The mathematical equation for the relative velocity of a uniform non-turbulent flow field is given by Equation 35, whereas, relative velocity of the incoming turbulent flow field is expressed in Equation 36.

$$U_{rel}^2 = U_{ref}^2 + \Omega r^2 = U_{ref}^2(1 + \lambda^2) \tag{35}$$

$$U_{rel}^2 = \left(U_{ref} + u'\right)^2 + (\Omega r + v')^2 \simeq U_{ref}^2 + u'^2 + (\Omega r)^2 + v'^2 \tag{36}$$

Brand et al. (2011) reported that the wind flowing towards a wind turbine is already turbulent, and in the process of extracting energy from the turbulent wind creates additional turbulence. Atmospheric turbulence impact wind energy through power performance, impacts on turbine loads, fatigue and wake effects as well as noise propagation. Therefore, Understanding and considering turbulence before and behind a wind turbine is believed to be vital in turbine applications (Mücke et al., 2010). The aerodynamic power is a function of the rotor shaft torque and the rotor speed upon which turbulence evolve. Atmospheric turbulence therefore gives rise to variations in the energy derived, power and consequently the electricity produced. In addition, turbulence is believed to be very instrumental in assessing energy yield in wind turbine applications (Gottschall & Peinke, 2008).

Results and Discussion
Vortex and Velocity Cut Plots
The following diagrams (Figure 7-10a-b) show the vortex flow and the velocity cut plots simulated at different wind speeds, while power and wake properties are examined. The simulation data from the turbine LLT simulation coupled with the different wind fields previously simulated are applied. A rotor overhang length of 0.6m and a hub height of 15m was used. The upwind type simulation was selected; the rotor shaft tilt was set at 5 deg in the downward direction. A TSR of 5 was selected for all scenarios and the simulation was run for 10s time steps. The results were read after 6s. From Fiure 7a, It can be

observed that as the flow progressed the velocity of wind along the axis of the turbine decreased steadily. As shown in Figure 7b, It can also be seen that wake shedding began to occur at about halfway across the cut plane at 4s. At 6s, it can be observed that the wind flow became more developed. The power was found to reduce by 0.1% per every 2s. The coefficient of power was 0.560359 and the power obtained was 0.041903Kw as shown in Figure 7b.
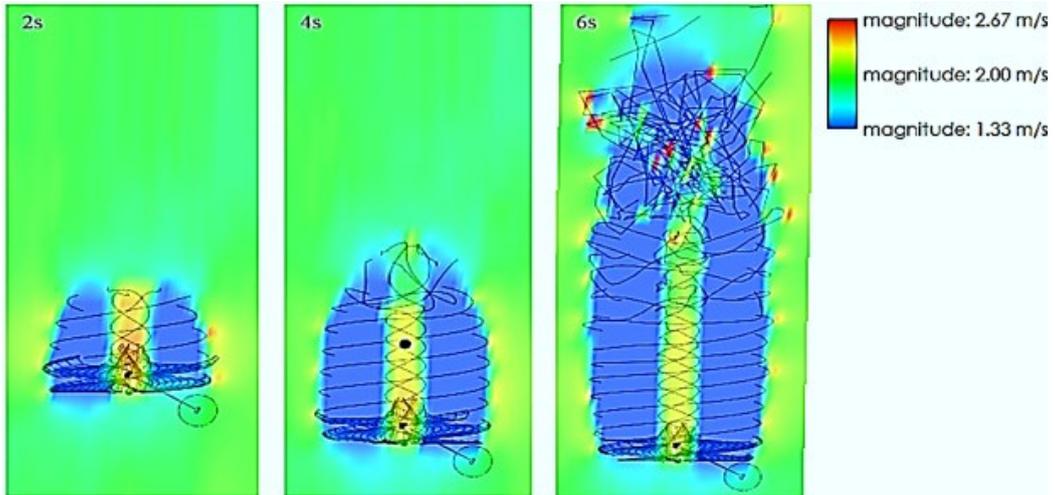
Figure 7a. Velocity cut plots at 2m/s after 2s, 4s and 6s
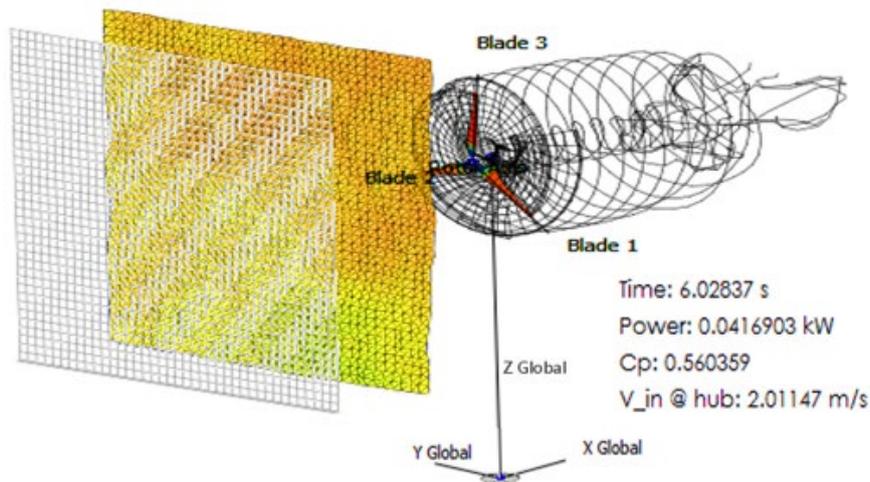
Figure 7b. Simulated profile of wake vortex trajectories at 2m/s.
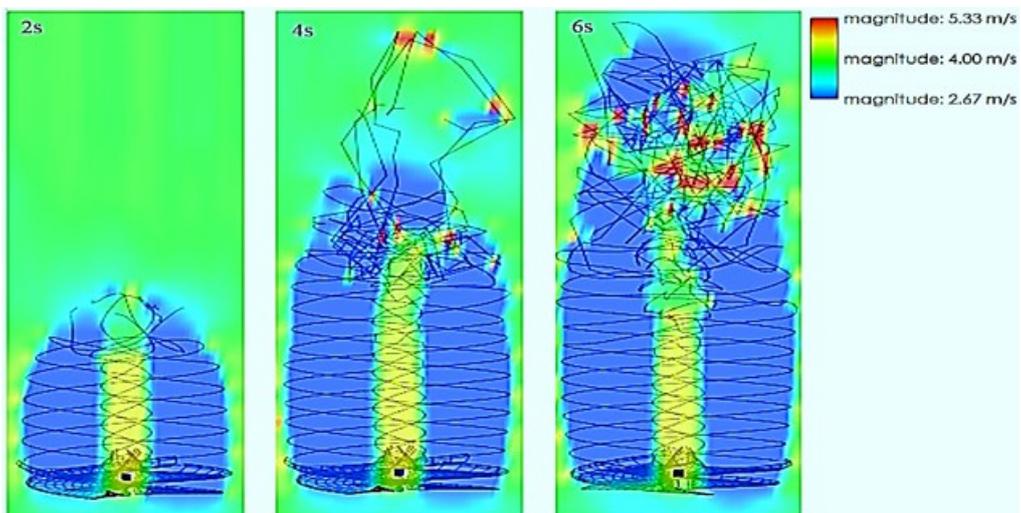
Figure 8a. Velocity Magnitude cut plots at 4m/s after 2s, 4s and 6s
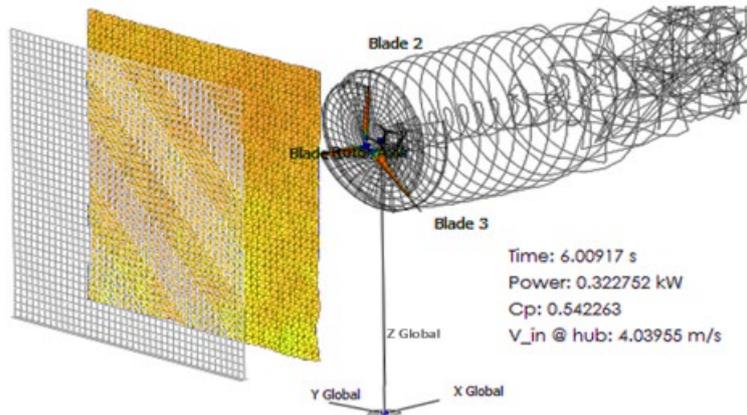
Figure 8b. Simulated profile of wake vortex trajectories at 4 m/s

From Figure 8a, It can be seen that the flow is uniform at 4s just as shear begins. The reduction in power is noticed in the third plot as it can be seen that the flow uniform length have reduced. The V_{in} and V_{out} is observed to increase due to an increase in the windspeed compared with the velocity plot at 2m/s. The power output is found to increase to 0.3228KW as shown in Figure 8b. The drop in power extracted from the wind to 0.54226 can be attributed to increased shedding and higher turbulence causing an overall decrease in turbine thrust. From Figure 9a, the cut plots show greater wake shedding and turbulence at 4s compared to the velocity plots at 4m/s. The velocity magnitude in Figure 9a is observed to reduce uniformly in the flow as well as the coefficient of power when compared to previous plots. The coefficient of power is 0.48407 and the power is found to be 0.96503Kw as presented in Figure 9b.
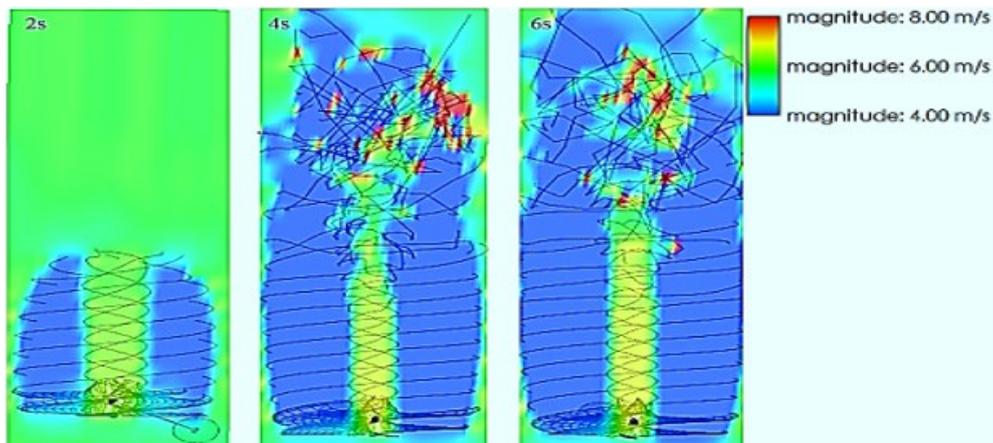
Figure 9b. Velocity Magnitude cut plots at 6m/s after 2s, 4s and 6s
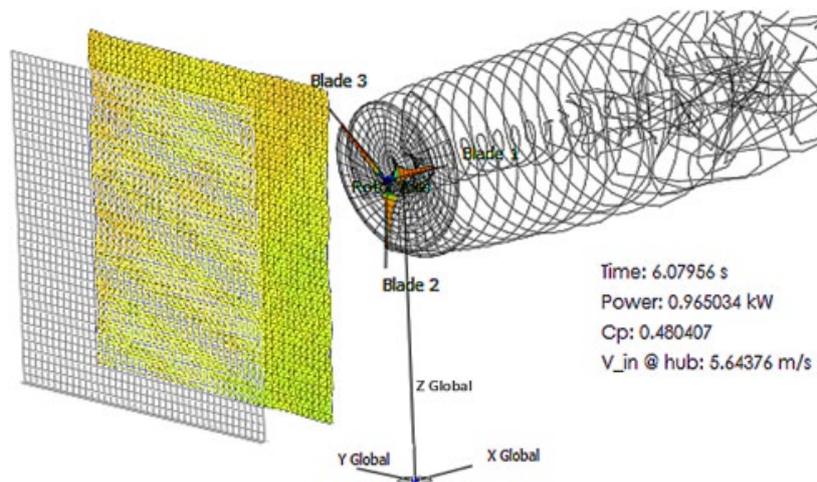
Figure 9a. Simulated profile of wake vortex trajectories at 6m/s

From Figure 10a, the wind turbulence at this wind speed (8m/s) is highly increased, but it can be noticed that the uniform flow length is greater than previous plots. This results in the increase in C_p to 0.5279 and power output to 2.514Kw as shown in Figure 10b. Figure 11 represents a plot of power coefficient and power output against wind speed. It can be observed from the plot that the power coefficient is not coherent with the wind speed possibly as a result deviation in the direction of wind by extreme effect of turbulence, whereas, the power output is coherent with the wind speed.
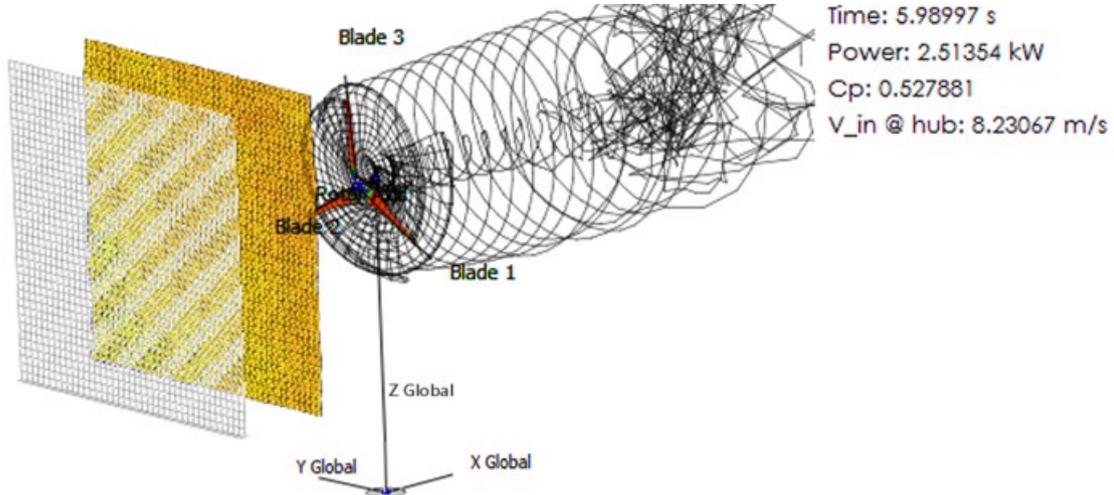
Figure 10a. Simulated profile of wake vortex trajectories at 8m/s
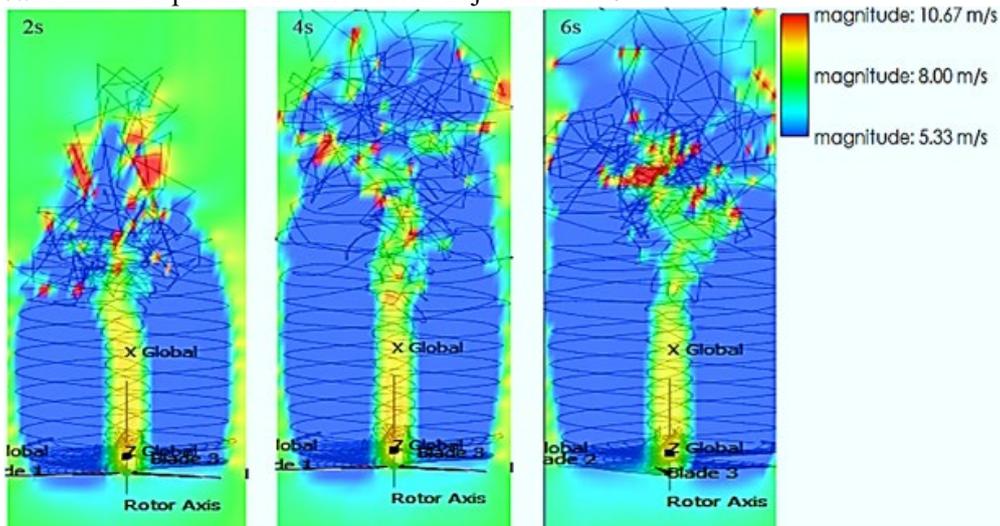
Figure 10b. Velocity Magnitude cut plots at 8m/s after 2s, 4s and 6s
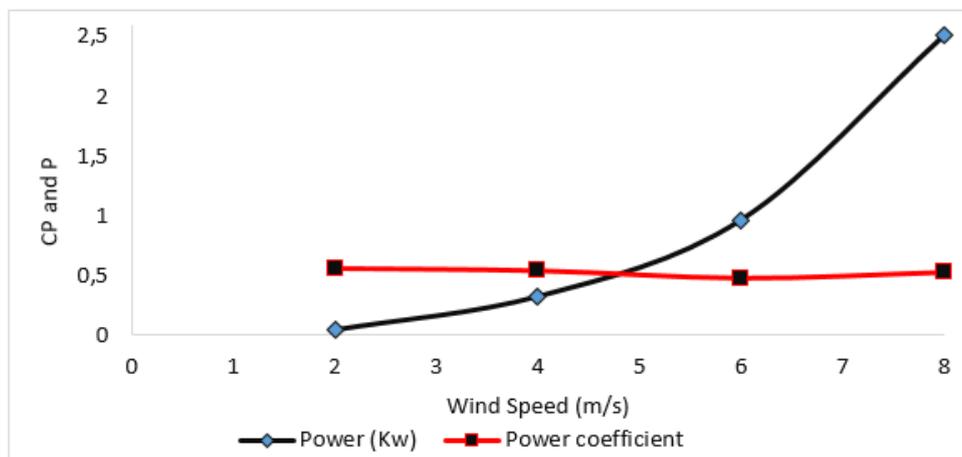
Figure 11. Plot of CP and P Vs wind speed

Conclusion

Increasing the number of points or time steps in the simulation resulted in much larger computational times and less computational errors. Furthermore, computational domain of atmospheric wind flow is very large and complex, thus, requires very large number of computational meshes. The results of the simulation revealed an increasing trend in power output (0.0416903, 0.322752, 0.965034 and 2.51354 kw) at increasing wind speeds (2, 4, 6 and 8 m/s) and varying trend in power coefficient (0.560359, 0.542263, 0.480407and 0.527881) at the same increasing wind speeds. The velocity magnitude cut plots simulated for the same range of wind speeds and time steps (2, 4 and 6 s) indicate that, failure of the wind velocity to attain optimum magnitude can affect the power coefficient as well as the energy available in the wind for extraction. In other words, if the wind flow, aerodynamic and turbine conditions are appropriate, the wind velocity can increase from few seconds or minutes, up to optimum magnitude suitable to impact on the rotors and cause rotation. The 3 dimensional spatial turbulent wind distribution patterns presented in this study shows that, turbulence in wind flow is characterised by wave patterns in all degrees of rotation of the turbine blade, and at extreme condition can distort the direction of wind flowing towards the rotors.

References

Kim D, Kim B, (2012) Development and validation of Computational Wind Field Model (Wind scape). Proceedings of 4th Asian Joint Workshop on Thermophysics and Fluid Science, October, 14-17, Busan, Korea.

Brand AJ, Peinke J, Mann, J, (2011) Turbulence and Wind Turbines. 13th European Turbulence Conference, Journal of Physics: Conference Series, 318(072005).

Satoh M, (2004) *Atmospheric circulation dynamics and general circulation models*. Springer. ISBN 3-540-42638-8.

Mikkelsen K, (2013) Effect of free stream turbulence on wind turbine performance. Norwegian University of Science and Technology, EPT-M-2013-84.

Li L, Liu Y, Yuan Z, Gao Y, (2018) Wind field effect on the power generation and aerodynamic performance of offshore floating wind turbines. Department of Naval Architecture, Ocean and Marine Engineering, University of Strathclyde, UK.

Ainslie J, (1988) Calculating the flowfield in the wake of wind turbines. *Journal of Wind Engineering and Industrial Aerodynamics,* **27**(1), 213-224.

Jimenez A, Crespo A, Migoya E, Garcia J (2007) Advances in large-eddy simulation of a wind turbine wake. Journal of Physics: Conference Series, 75, 012041, August, 28-31, Denmark.

Troldborg N, Sørensen JN, Mikkelsen R, (2010) Numerical simulations of wake characteristics of a wind turbine in uniform inflow. *Wind Energy* 13(1), 86-99.

Troldborg N, Larsen GC, Madsen HA, Hansen KS, Sørensen JN, Mikkelsen R, (2011) Numerical simulations of wake interaction between two wind turbines at various inflow conditions. *Wind Energy* **14**(7), 859-876.

Sanderse B, (2000) Aerodynamics of Wind Turbine Wakes. Technical Report ECN-E-09-016, Energy research centre of the Netherlands, Netherlands.

Wußow S, Sitzki L, Hahm T, (2007) 3D-simulation of the turbulent wake behind a wind turbine. Journal of Physics: Conference Series, 75, 012033, August, 28-31, Denmark.

Zhang W, Markfort CD, Porte-Agel F, (2012) Near-wake flow structure downwind of a wind turbine in a turbulent boundary layer. Springer, *Experiments in Fluids*, 52, 1219-1235.

Ozbay A, Tian W, Hu H, (2016) Experimental Investigation on the Wake Characteristics and Aeromechanics of Dual-Rotor Wind Turbines. *Journal of Engineering for Gas Turbines & Power,* **138**(042602), 1-15.

Tian W, Ozbay A, Hu H, (2014) Effects of Incoming Surface Wind Conditions on the Wake Characteristics and Dynamic Wind Loads Acting on a Wind Turbine Model. *Physics of Fluids,* **26**(12), 5108.

Hu H, Yang Z, Sarkar P, (2012) Dynamic Wind Loads and Wake Characteristics of a Wind Turbine Model in an Atmospheric Boundary Layer Wind. *Experiments in Fluids,* **52**(5), 1277-1294.

Whale J, Anderson CG, Bareiss R, Wagner S, (2000) An Experimental and Numerical Study of the Vortex Structure in the Wake of a Wind Turbine. *Journal of Wind Engineering and Industrial Aerodynamics,* **84**(1), 1-21.

Sørensen JN (2011) Aerodynamic aspects of wind energy conversion. *Annual Review of Fluid Mechanics,* 43, 427-448.

Devinant PH, Laverne T, Hureau J, (2002) Experimental study of wind turbine airfoil aerodynamics in high turbulence. *Journal of Wind Engineering and Industrial Aerodynamics,* **90**(6), 689-707.

Fukumoto Y, Okulov VL (2005) The velocity field induced by a helical vortex tube. *Physics of Fluids,* **17**(10), 107101.

Zheng ZC, Wu H, (2018) Classification of Wind Farm Turbulence and Its Effects on General Aviation Aircraft and Airports. University of Kansas, Report No. K-TRAN: KU-16-3.

Mulinazzi TE, Zheng ZC, (2014) Wind farm turbulence impacts on general aviation airports in Kansas (K-TRAN: KU-13-6). Topeka, KS: University of Kansas.

Odemark Y (2012) Wakes behind wind turbines-Studies on tip vortex evolution and stability. Royal Institute of Technology, SE-100 44 Stockholm, Sweden.

Manwell JF, McGowan JG, Rogers AL, (2009) *Wind Energy explained*, 2nd Edition, Wiley.

Vermeer L, Sorensen J, Crespo A, (2003) Wind Turbine Wake Aerodynamics. *Progress in Aerospace Sciences*, **39**, 467-510.

Mckay P, Carriveau R, Ting D, Newson T, (2012) Turbine Wake Dynamics, Advances in Wind Power. IntechOpen Limited, London, EC3R 6AF, United Kingdom.

Marmidis G, Lazarou S, Pyrgioti E, (2008) Optimal placement of wind turbines in a wind park using Monte Carlo simulation. *Renewable Energy,* **33**, 1455-1460.

McKay P, Carriveau R, Ting DS, (2011) Farm Wide Dynamics: The Next Critical Wind Energy Frontier. *Wind Engineering,* 35(4), 397-418.

Burton T, Sharpe D, Jenkins N, Bossanyi E, (2001) *Wind Energy Handbook.* John Wiley & Sons Ltd, Chichester.

Li L, Wang Y, Liu Y, (2017) Impact of wake effect on wind power prediction. State Key Laboratory of Alternate Electrical Power System with Renewable Energy Sources, North China Electric Power University, Beijing, 102206, China.

Kaimal JC, Wyngaard JC, Izumi Y, Coté OR, (1972) Spectral characteristics of surface layer turbulence. *Quarterly J. Royal Meteorological Society,* **98**(417), 563-589.

Veers PS, (1984) Three-dimensional wind simulation. Technical report SAND88-0152, Sandia National Laboratories.

Mann J, (1998) Wind field simulation. *Probabilistic Engineering Mechanics,* **13**(4), 269-282.

Mücke T, Kleinhans D, Peinke J, (2010) Atmospheric turbulence and its influence on the alternating loads on wind turbines. *Wind Energy,* 14(2), 301-316.

Gottschall J, Peinke J, (2008) How to improve the estimation of power curves for wind turbines. *Environmental Research Letters,* **3**(1), 015005, 1-7.